ELSEVIER

International Journal of Pharmaceutics 224 (2001) 131–140

international journal of pharmaceutics

www.elsevier.com/locate/ijpharm

# Application of fractal geometry to dissolution kinetic study of a sweetener excipient

A. Tromelin *, G. Hautbout, Y. Pourcelot

*Groupe Technologie des Poudres à Usage Pharmaceutique, Faculté de Pharmacie, Université de Bourgogne, 7 boulevard Jeanne d'Arc, 21033 Dijon, France*

Received 11 October 2000; received in revised form 16 May 2001; accepted 23 May 2001

**Abstract**

In the context of relationship study between dissolution kinetic and particle morphology using the fractal geometry tool, we use a commercially available quality of saccharin powder. The characterization of molecular feature and image analysis study allows us to conclude to the statistic self-similarity of particles of four sieved particles size fractions, permitting the fractal approach. Calculation of reactive fractal dimension is performed using two forms of mass transfer equation: $-\mathrm{d}Q/\mathrm{d}t = kQ^{D_R/3}\Delta C$ and $-\mathrm{d}Q/\mathrm{d}t = k'R^{D_R-3}\Delta C$, with $\Delta C = \{C_f/[\ln C_s/(C_s - C_f)]\}$. Based on comparison of the surface fractal dimension $D_S$ on the two values of reactive fractal dimension $D_R$, a dissolution mechanism can be drawn: the dissolution starts at the whole surface of particles and is further governed by digging into holes that involve inner mass of particles. S.E.M. observations confirm this hypothesis. The confrontation between the $D_R$ values provided by the two ways of determination is essential for a good prediction of the mechanism.


*Keywords:* Dissolution kinetic; Fractal geometry; Saccharin; Sweetener excipient

## 1. Introduction

For some 15 years the concept of fractals has been used in order to describe the process of erosion of fine particles (Kaye et al., 1985). More recently, the fractal geometry is also applied in the study of morphology of reactive surface involved in the dissolution mechanism of a drug (Farin and Avnir, 1992, 1987; Fernandez-Hervas et al., 1994; Tromelin et al., 1996). In our earlier investigation (Tromelin et al., 1996), we exploited the use of two forms of the Noyes–Whitney equation proposed by Farin and Avnir (1992) according to Wenzel's law. Our study is performed on a mineral substance, the orthoboric acid, chosen as a model of a water-soluble powder.

In our present work, we selected an organic compound as powder model and pseudo-drug, the saccharin, sweetener excipient used in the pharmaceutical domain. The choice of saccharin among sweetener is controlled by several consid-

* Corresponding author. Tel.: +33-3-8039-3214; fax: +33-3-8039-3300.

*E-mail address:* anne.tromelin@u-bourgogne.fr (A. Tromelin).

0378-5173/01/$ - see front matter 
PII: S0378-5173(01)00743-8

erations on desirable advantages. The crystal network is well known (monoclinic), the powder is stable at room temperature (melting point 229 °C), little expensive, the granulometric distribution of commercial powder is between 50 and 300 μm and the solubility in water is from 0.1 to 0.01 mol $l^{-1}$ ($C_s = 0.024$ mol $l^{-1}$ at 37 °C).

The aim of our present study is the proposal of a dissolution mechanism based on the comparison of surface fractal dimension $D_S$ provided from specific surface measurement and fractal reactive dimension $D_R$ which is obtained from Eqs. (1) and (2) (Farin and Avnir, 1992).

$$-\frac{dQ}{dt} = kQ^{D_R/3}(C_S - C) \quad (1)$$

For each granulometric fraction, $D_R$ is calculated from the slope of ln (dissolution rate) versus ln (non dissolved product amount).

$$-\frac{dQ}{dt} = k'R^{D_R-3}(C_S - C) \quad (2)$$

where $R$ is the particle mean diameter for narrowly sieved fractions. The selected kinetic parameters are the highest value of dissolution rate for each granulometric fraction. $k$ and $k'$ are constants dependent on the hydrodynamic conditions and cell volume.

Characterisation of molecular and particular aspects is carried out of four sieved particle size fractions (63–100, 100–150, 150–200 and 200–250 μm) in order to probe the self-similarity, which allows the fractal approach. This observation is supported by the study of shape factors distribution provided by image analysis data.

Dissolution data are fitted to the Weibull function:

$$F(t) = a\ (1 - \exp(-b(t-d)^c)) \quad (3)$$

from which derivative provides calculated values of dissolution rate.

Moreover, in order to confirm the proposed mechanism, S.E.M. observations are carried out on particles before dissolution and at 50% of dissolution. In order to obtain reliable partially dissolved particles, we use glass flow-through dissolution cell adapted to allow fast of dissolution medium removing.

## 2. Materials and methods

### 2.1. Materials

We use four sieved granulometric fractions of available commercial grade saccharin powder (Aldrich DAB8 ref 10.918-5 lot 04455-076): 63–100, 100–150, 150–200 and 200–250 μm). Preparative sieving is carried out using air jet separator 200LSN (Hosokawa Alpine).

### 2.2. Characterization

#### 2.2.1. X-ray diffraction

X-ray diffraction is performed using CPS 120 INEL diffraction system fitted with a localization curve-Cu-anti cathode (120°, 4096 channels).

#### 2.2.2. Density measurement

Density measurement is carried out using helium pycnometry (Quantachrom Multipycnometer). After 70 cycles to reach thermal equilibrate, 30 cycle of measure are performed.

#### 2.2.3. Image analysis

Image analysis is performed on a system composed of an optical microscope Nachet NS 400 (lens × 8, × 16), linked to a Cohu camera (4712-5000). The samples are prepared so that the particles are well separate by suspension in castor oil. The particle image is digitalized (1 pixel/μm) using a VIDAS computer program (Kontron on PC 386-387). Image analysis is carried out without using macro function or filter. After binarisation, the function 'scrap' of VIDAS computer program is used in order to remove the images of background noise fictitious particles. Treatment of the data is performed using Excel software. The determination of size and shape of the particles is carried out using 100 particles of each fraction (Paine, 1993).

The used shape factors are—(1) Earlier measurement (Yasuo and Kikuo, 1991), $d_{max}$ = maximum Feret diameter; $d_{min}$ = minimum Feret diameter; $A$ = measured surface area; Perim = measured perimeter; $C_{Perim}$ = perimeter of polygon including the particle image (polygon regular convex of 32 sides for Vidas software). (2)

Shape factors (Brewer and Ramsland, 1995), Elongation = $d_{max}/d_{min}$; Roundness = $4A/\pi d_{max}^2$; Circularity = $4\pi A/Perim^2$; Roughness = $Perim/C_{perim}$.

### 2.2.4. S.E.M. observations

S.E.M. observations (Jeol JSM-6400F) are executed on particles of the four fractions 63–100, 100–150, 150–200 and 200–250 μm before dissolution and on particles isolated as described further at 50% of dissolution. In order to avoid electric load of surfaces, particles are coated with thin gold film (30 nm). This film is obtained with gold vapour condensation on particles surface. Heating by Joule effect of gold in tungsten basket at 1300 °C under *vacuum* ($10^{-4}$ mbar) produces the vapour.

### 2.2.5. Adsorption

The specific surface area measurement of particle size classes is carried out using the BET method with krypton as adsorbent (Autosorb-1 Quantachrom). The degassing is carried out under *vacuum* at ambient temperature until pressure become stable (about 2 h under 5 mTorr).

The fractal dimension of particle surface area $D_S$ is calculated from the slope of the Richardson plot of ln ($S$) versus ln ($R$), where $R$ is the mean radius of each size fraction.

## 2.3. Dissolution study

### 2.3.1. Dissolution testing

Dissolution testing is carried out in a glass flow-through cell (Tingstad and Riegelman, 1970), 40 mm long and a 17 mm in internal diameter, and having a 18 ml volume. The cell is constituted of two glass filter funnels equipped with sintered glass filter at one of extremities and threaded at other extremity. These two tubes are connected back to back with bridge SVL22. Three-way stopcock is used in order to allow fast remove of dissolution medium (Fig. 1). During testing, the dissolution medium (purified water with 0.01% lauryl sulfate sodium) circulates by pumping (pump CY1D, SOTAX) through the cell at a fixed flow rate of 30 ml $min^{-1}$. The aqueous dissolution medium is maintained at 37 °C using a water bath (Polystat 22 Bioblock). Sampling are took at 20 s for the first five samples, at 30 s for the four followings, at every minute up to 4 min and then at every other minute up to end. Three essays are carried out for each granulometric fraction.

The concentration of each aliquot is diluted at 1/25 is determined using spectrophotometric dosage at 267.3 nm using linear regression equation $y = 1.537x + 0.0082$ ($r^2 = 1.00$; Confidence interval (CI) = $\pm 0.084$ for $\alpha = 5\%$), where $x$ is the optical density and $y$ the concentration (mmol $l^{-1}$).

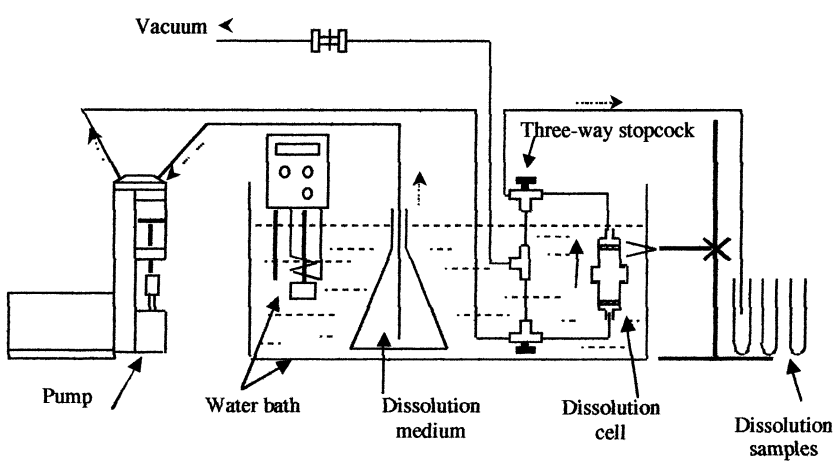


Fig. 1. Schema of dissolution apparatus.

The dissolution process is stopped at 50% of dissolution by the removal under vacuum of the dissolution medium at times determined on the basis of complete dissolution data (1 min 40 s, 2 min 10 s, 2 min 30 s and 3 min for 63–100, 100–150, 150–200 and 200–250 μm granulometric fraction, respectively).

*2.3.2. Fitting of dissolution rate*

For the approximation of dissolution data $Q_d = F(t)$, we use Weibull (Elkoshi, 1997) function Eq. (3′):

$$F(t) = a\ (1 - \exp(-b(t-d)^c)) \qquad (3')$$

The function fitting is carried out using the 'Curve Fit' command from the 'Math' menu of Sigma Plot software. This command fits data to non-linear functions using an iterative process to find parameters for the equation that best fit the data

The values of dissolution rate versus times are then given by the derivative function Eq. (4):

$$\frac{dF(t)}{dt} = abc \exp(-b\ (t-d)^c)\ (t-d)^{c-1} \qquad (4)$$

*2.3.3. Mass transfer equation*

The dissolution is performed in flow-through cell in 'non-sink' conditions so that $C_f < 0.1C_S$. When 'sink' conditions are not performed, it is impossible to neglect $C_f$ in comparison with $C_s$. According to these experimental conditions we use the following mass transfer Eq. (5) (Frolov, 1998):

$$-\frac{dQ}{dt} = KS\Delta C \quad \text{with } \Delta C = \frac{C_f}{\ln C_s/(C_s - C_f)} \qquad (5)$$

*2.3.4. The reactive fractal dimension*

The reactive fractal dimension of particles is calculated from the slope of the Richardson plot.

From Eq. (1)

$$\ln \frac{(dQ/dt)}{\Delta C} \text{ versus } \ln(Q)$$

From Eq. (2)

$$\ln \frac{(dQ/dt)_{max}}{\Delta C} \text{ versus } \ln(R)$$

Regression is calculated using data points of three experiments (except for the 200–250 μm fraction).

## 3. Results

### 3.1. Molecular characterization

From pycnometry helium measurements, the density values found for the four particles size classes 63–100, 100–150, 150–200 and 200–250 μm are: 1.5774 ($CI = \pm 2 \times 10^{-4}$ for $\alpha = 5\%$), 1.5775 ($CI = \pm 5 \times 10^{-5}$ for $\alpha = 5\%$), 1.5757 ($CI = \pm 6 \times 10^{-5}$ for $\alpha = 5\%$) and 1.5750 ($CI = \pm 10^{-4}$ for $\alpha = 5\%$), respectively. These values indicate the chemical identity of the four particles size classes.

Analysis of the diffractogram obtained for the four granulometric fractions 63–100, 100–150, 150–200 and 200–250 μm shows that the crystalline states are similar and displays no detectable amorphization level (Fig. 2). The difference of ray's intensities is attributable to the different orientations of crystal.

### 3.2. Particular characterization

From microscopic observations and image analysis data, the statistic parameters of shape factors distribution (elongation, roughness, circularity and roundness) of the four fractions are reported in Table 1.

S.E.M. micrographs show particles of the 150–200 μm particle size class before dissolution (Fig. 3A) and isolated at 50% of dissolution (Fig. 3B) and particle of the 100–150 μm fraction isolated at 50% of dissolution (Fig. 4A, B).

### 3.3. Self-similarity condition

The molecular structure study shows that the four granulometric fractions are related to the same crystal network. The application of fractal geometry in dissolution study requires the use of narrowly sieved fractions of powder, because ideal conditions, i.e. the use of identical size particles

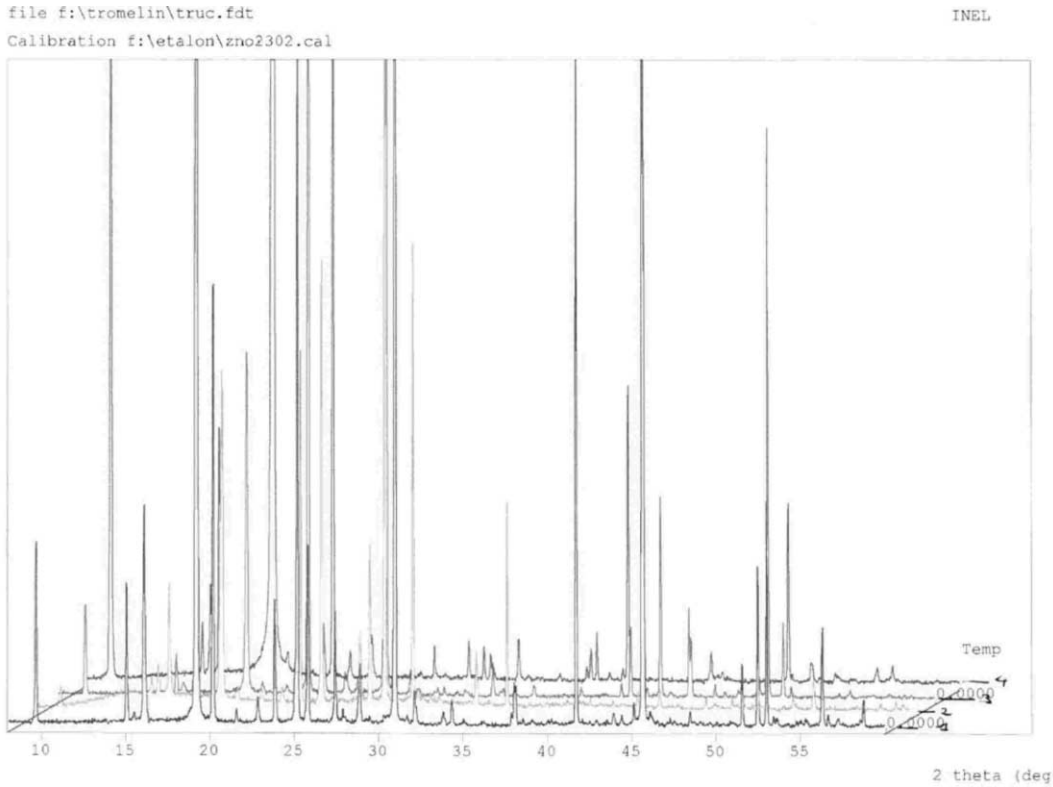


Fig. 2. R.X. diffractogram for the four granulometric fractions.

are not practically workable. For this reason, diameters distribution must be centered and symmetric, corresponding to close values for mean and mode of diameters distribution. The image analysis work points out that the values of each shape parameters are very close for the four granulometric fractions. On the basis of the results of both molecular structure and characterization of morphological properties we can conclude to the statistical self-similarity of particles.

### 3.4. Dissolution study

#### 3.4.1. Dissolution testing

Experimental dissolution profiles show that the reproducibility of the essays is satisfactory. For each granulometric fraction and for the used time interval, the coefficient of variation is smaller than 15%.

#### 3.4.2. Fitting of dissolution curve

For one essay on the 100–150 μm fraction, chosen as example, experimental and fitted curves for cumulative profiles of dissolution is depicted in Fig. 5A. From the fitted function, the mathematical derived provided calculated values of dissolution rate. The calculated differential profile is close, but not exactly the same, that experimental profile; indeed, experimental values of 'dissolution rate' are in fact values of $\Delta Q_d/\Delta t$, with $\Delta t \to 0$, but limited by experimental conditions ($\Delta t \sim 20$ s at the beginning of the dissolution) (Fig. 5B). Calculated dissolution rate values Eq. (4) are used in the following determination of reactive fractal dimension.

Table 1
Statistic parameters of shape factors distribution (S.E. in parentheses)

| | Shape parameters | 63–100 μm | 100–150 μm | 150–200 μm | 200–250 μm |
|---|---|---|---|---|---|
| Mode | D equivalent Surf (μm) | 110 | 140 | 170 | 260 |
| | Elongation | 1.30 | 1.45 | 1.45 | 1.45 |
| | Roughness | 1.30 | 1.30 | 1.30 | 1.30 |
| | Circularity | 0.75 | 0.75 | 0.75 | 0.65 |
| | Roundness | 0.75 | 0.70 | 0.70 | 0.70 |
| Mean | D equivalent Surf (μm) | 96 (2) | 124 (3) | 159 (4) | 246 (6) |
| | Elongation | 1.44 (0.03) | 1.41 (0.02) | 1.45 (0.02) | 1.50 (0.03) |
| | Roughness | 1.26 (0.01) | 1.30 (0.01) | 1.31 (0.02) | 1.33 (0.02) |
| | Circularity | 0.69 (0.01) | 0.68 (0.01) | 0.65 (0.01) | 0.65 (0.01) |
| | Roundness | 0.67 (0.01) | 0.66 (0.01) | 0.64 (0.01) | 0.62 (0.01) |

### *3.5. Determination of fractal dimension*

#### *3.5.1. Surface fractal dimension*

Specific surface areas, $S_g$ measurements for the six narrowly sieved fractions 0–38, 38–63, 63–100, 100–150, 150–200 and 200–250 μm are 0.27, 0.14, 0.0626, 0.104, 0.072 and 0.046 $m^2\ g^{-1}$, respectively. According to $S_g \propto R^{D_s-3}$, the fractal dimension $D_s$ is calculated as a function of particle size classes mean radius from the slope of the Richardson plot and is found equal to 2.30 (Table 2).

#### *3.5.2. Determination of reactive fractal dimension*

*3.5.2.1. From Eq. (1):* $v \propto Q^{D_R/3}$. The Richardson plot of the dissolution profile $\ln (dQ/dt)_{calc}$ versus $\ln (Q)$ obtained with the 100–150 μm fraction is displayed as example in Fig. 6. The choice regression domain is restricted to the linear segment of Richardson plot (Tromelin et al., 1996), that is the domain comprising between 20 and 90% of dissolution. Regression parameters for the $D_R$ determination are listed in Table 3. The minimum and maximum $D_R$ values are founded equal to 2.99 and 3,79 for the 63–100 μm fraction, 2.68 and 2.88 for the 100–150 μm fraction, 2.55 and 3.05 for the 150–200 μm fraction, 2.89 and 2.96 for the 200–250 μm fraction.

*3.5.2.2. From Eq. (2):* $v \propto R^{D_R-3}$. For each granulometric fraction, the determination of $D_R$ is carried out using $v_{max}$, which is the highest calculated dissolution rate.

The regression parameters for calculation of $D_R$ values are reported in Table 4. The calculated value of $D_R$ is 2.28.

## 4. Discussion

Scanning electron microscopic observations for the four granulometric fraction show bulk particles with smooth surfaces but also some irregularity as holes, as it appears in Fig. 3A for the 150–200 μm fraction. The $D_S$ value of 2.30 provided by measurement of specific surface area indicates the presence of few irregularities and is consistent with S.E.M. observations.

The S.E.M observations at 50% of dissolution reveal that the contours of particles become smoother, but ridges become visible and both the number and the dimension of holes increase (Fig. 3B).

Table 2
Regression parameters obtained in the $D_S$ study from specific surfaces

| | |
|---|---|
| $R^2$ | 0.7867 |
| S.E. of estimate | 0.3285 |
| Slope | −0.7046 |
| CI of slope ($\alpha = 5\%$): min value; max value | −1.214; −0.1954 |
| S.E. | 0.1834 |
| $T$ | 3.842 |
| $F$ test | 14.76 |
| $F$ critical | 7.709 |
| Probability | 0.01844 |
| Observations | 6 |

Table 3
Regression parameters obtained in the $D_R$ study from Eq. (1)

| | Fraction 63–100 μm | | | Fraction 100–150 μm | | | Fraction 150–200 μm | | | Fraction 200-250 μm | |
|---|---|---|---|---|---|---|---|---|---|---|---|
| | Essay 1 | Essay 2 | Essay 3 | Essay 1 | Essay 2 | Essay 3 | Essay 1 | Essay 2 | Essay 3 | Essay 1 | Essay 3 |
| $R^2$ | 0.9932 | 0.9988 | 0.9924 | 0.9902 | 0.9922 | 0.9936 | 0.9956 | 0.9943 | 0.9849 | 0.9969 | 0.9915 |
| S.E. | 0.0634 | 0.0338 | 0.1068 | 0.0655 | 0.0511 | 0.0587 | 0.0409 | 0.0563 | 0.0720 | 0.0243 | 0.0526 |
| Slope | 0.9753 | 1.239 | 1.264 | 0.9055 | 0.8944 | 0.9613 | 0.8515 | 1.0152 | 0.9183 | 0.9883 | 0.9620 |
| CI ($\alpha = 5\%$) × : Min value; max value | 0.9143; 1.036 | 1.207; 1.272 | 1.181; 1.348 | 0.8421; 0.9689 | 0.8384: 0.9505 | 0.9071; 1.016 | 0.8114; 0.8915 | 0.9610; 1.069 | 0.8382; 0.9984 | 0.9471; 1.030 | 0.8947; 1.029 |
| S.E. | 0.02698 | 0.01435 | 0.03695 | 0.02846 | 0.02516 | 0.02432 | 0.01796 | 0.02432 | 0.03594 | 0.01823 | 0.02975 |
| $T$ | 36.15 | 86.36 | 34.22 | 31.82 | 35.55 | 39.53 | 47.40 | 41.75 | 25.55 | 54.23 | 32.34 |
| $F$ test | 1307 | 7459 | 1171 | 1013 | 1264 | 1563 | 2247 | 1743 | 653 | 2940 | 1046 |
| $F$ critical | 5.1 | 5.1 | 5.1 | 5.0 | 5.0 | 5.0 | 5.0 | 5.0 | 5.0 | 5.1 | 5.1 |
| Probability | 4.692E-11 | 1.896E-14 | 7.678E-11 | 2.211E-11 | 7.352E-12 | 2.565E-12 | 4.213E-13 | 1.491E-12 | 1.937E-10 | 1.240E-12 | 1.271E-10 |
| Observations | 11 | 11 | 11 | 12 | 12 | 12 | 12 | 12 | 12 | 11 | 11 |

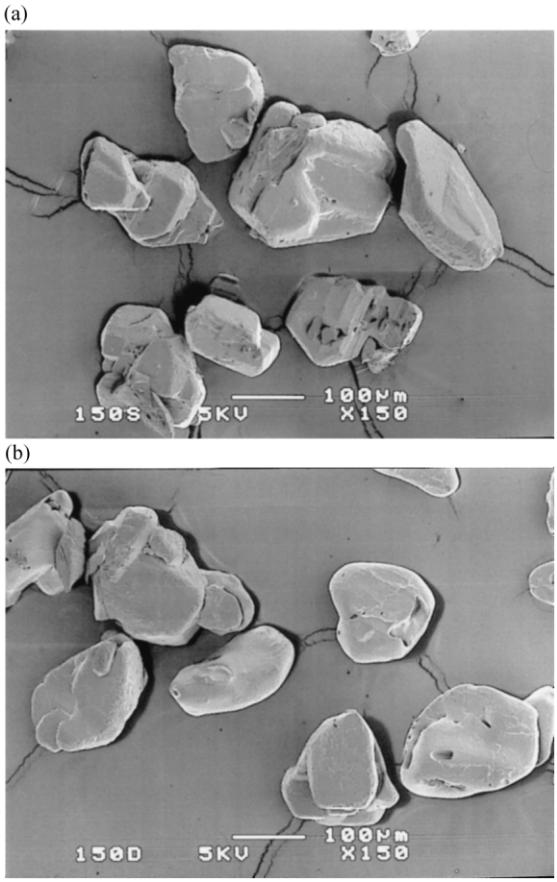


Fig. 3. Scanning electron micrographs of 150–200 μm fraction before dissolution (A) and at 50% of dissolution (B).

The calculation of $D_R$ by the Eq. (1) provided the values 2.55–3.79. Except of the 63–100 μm fraction, for which the values superior to three are difficult to interpret, these values are characteristic of rough surfaces.

According to Farin and Avnir (1992), $D_R > D_s$ indicates roughening of surface or trapping of the dissolution medium in pore volumes which can be due to diffusional limitations. One hypothesis is that the reaction occurs selectively at cracks of surface and continues by roughening at these sites; then the dissolution medium is trapped in these formed micropores or holes. In this context, the high values of 2.99–3.79 observed for the 63–100 μm granulometric fraction can be attributed to trapping of dissolution medium in very small holes.

The calculated value of $D_R$ by Eq. (2), using $v_{max}$, is 2.28. This value is very close to $D_S$ value (2.30). This case ($D_R \sim D_S$) can reflect that the reaction can occur at the whole surface. It can also represent two simultaneous phenomenons (Farin and Avnir, 1987), (i) roughening and/or trapping of dissolution medium in micropores, as describe before ($D_R > D_S$), (ii) diffusionnal inaccessibility of parts of surface or chemical selectivity due to heterogeneously distribution of activation energy ($D_R < D_S$). This hypothesis is consistent with our S.E.M. observations, which display some ridges at the surface and smoothing of edge, reflecting that the beginning of dissolution affect differently the whole surface of particles (Fig. 4A, B).

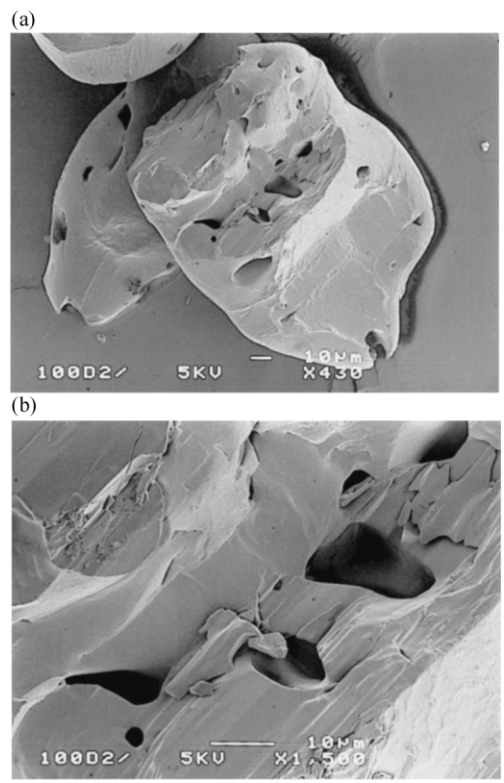


Fig. 4. Scanning electron micrographs of a particle of 100–150 μm size fraction at 50% of dissolution (A) and detail of surface (B).

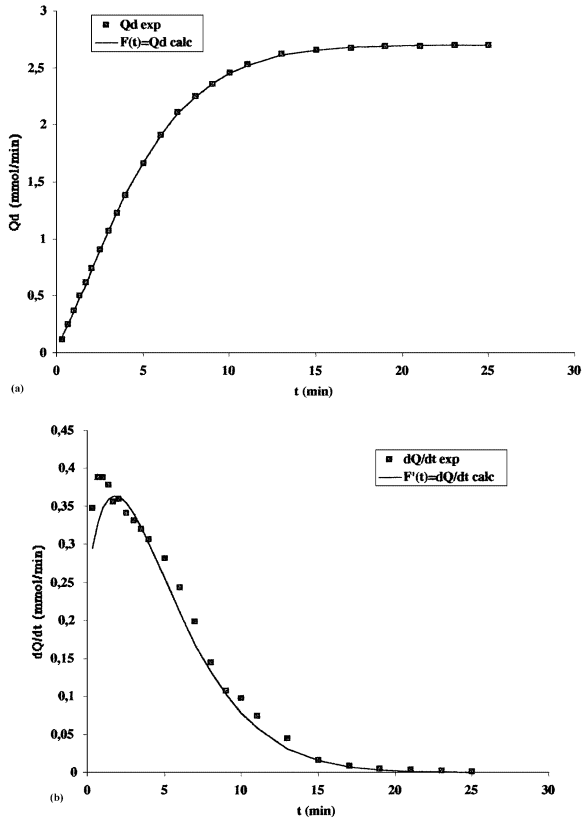


Fig. 5. For 100–150 μm fraction, (A) fitting of cumulative curve using Eq. (3) $F(t) = a(1 - \exp(-b(t-d)^c))$; (B) experimental and calculated differential profiles of dissolution.

The values of $D_R$ from Eqs. (1) and (2) are different or even contradictory and lead to different interpretations if they are comprehended separately. The values provided by Eqs. (1) and (2) are complementary and their confrontation to S.E.M. observations is necessary to attribute a dissolution mechanism. For this reason, only one way of determination provides some limited information on dissolution mechanism. On the basis of these whole results and according to the S.E.M observations, a hypothesis can be drawn. The dissolution starts at the whole surface of particles by roughening at several sites of surface and by smoothing at several other sites, and is further governed by the digging of holes, which develop inside the mass of particles.

We can underline that confrontation between the $D_R$ values provided by the two ways of determination and is essential for a good prediction of the mechanism. The use of fractal geometry appears to be a good tool only if $D_S$ value is confront with several values of $D_R$ which are characteristic of different states of dissolution.

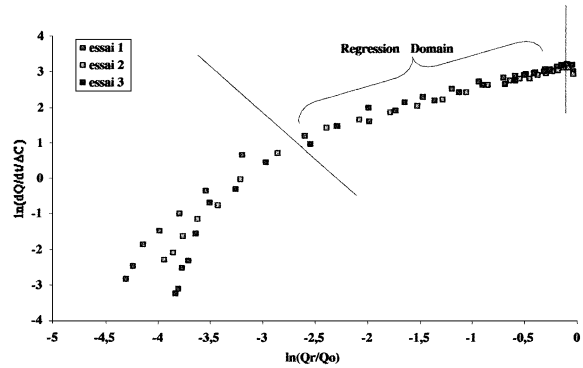


Fig. 6. Richardson plot of dissolution profile for 100–150 μm fraction.

## Acknowledgements

We gratefully thank Dr P. Bracconi for helpful discussions and his welcome in laboratories. Thanks are due to M.B. Berini, Engineer, for the specific surface measurements, to C. Josse, Engineer, for the S.E.M. study, to M. Mesnier, Engineer, who kindly carried out the X-ray diffraction spectra (Université de Bourgogne, Faculté de Sciences et Techniques, Laboratoire de Recherches sur la Réactivité des Solides), to M.X. Lelièvre for his work on dissolution studies, and to M.S. Mielcarek for his capable technique assistance. We would like to thank Dr C. Andrès for his contribution towards image analysis.

Table 4
Regression parameters obtained in the $D_R$ study from Eq. (2)

| | |
|---|---|
| $R^2$ | 0.75586 |
| S.D. of estimate | 0.1675 |
| Slope | −0.7206 |
| CI of slope ($\alpha = 5\%$): min value; max value | −1.029; −0.4118 |
| S.E. | 0.1365 |
| $T$ | 5.279 |
| $F$ test | 27.86 |
| $F$ critical | 5.117 |
| Probability | 5.080 E-4 |
| Observations | 11 |

## Appendix A. Nomenclature

| | |
|---|---|
| $a$, $b$, $c$, $d$, | calculated parameters by fitting of the Weibull function $F(t) = a(1 - \exp(-b(t-d)^c))$ |
| $C$ | dissolution medium concentration (mmol $l^{-1}$) |
| $C_f$ | final solution concentration (mmol $l^{-1}$) |
| $C_s$ | saturation concentration (mmol $l^{-1}$) |
| $D_R$ | dissolution fractal dimension |
| $D_S$ | fractal surface dimension |
| $Q$ | amount of non-dissolved product (mmol) |
| $Q_d$ | amount of dissolved product (mmol) |
| $R$ | radius of particle (μm) |
| $S$ | surface area of reactive surface ($m^2$) |
| $S_g$ | specific surface area ($m^2$ $g^{-1}$) |
| $T$ | time (min) |
| $V$ | $-dQ/dt$ = dissolution rate (mmol $min^{-1}$) |

## References

Brewer, E., Ramsland, A., 1995. Particle size determination by automated microscopical imaging analysis with comparison to laser diffraction. J. Pharm. Sci. 84, 499–501.

Elkoshi, Z., 1997. On the variability of dissolution data. Pharm. Res. 14, 1355–1362.

Farin, D., Avnir, D., 1987. Reactive fractal surfaces. J. Phys. Chem. 91, 5517–5521.

Farin, D., Avnir, D., 1992. Use of fractal geometry to determine effects of surface morphology on drug dissolution. J. Pharm. Sci. 81, 54–57.

Fernandez-Hervas, M.-J., Holgado, M.-A., Rabasco, A.-M., Fini, A., 1994. Use of fractal geometry on the characterization of particles morphology: application to the diclofenac hydroxyethylpirrolidine salt. Int. J. Pharm. 108, 187–194.

Frolov, V.F., 1998. Dissolution of disperse materials. Theor. Found. Chem. Eng. 32, 357–368.

Kaye, B.H., Leblanc, J.E., Abbot, P., 1985. Fractal description of the structure of fresh and eroded aluminum shot fine particles. Part. Charact. 2, 56–61.

Paine, A.J., 1993. Error estimates in the sampling from particle size distribution. Part. Part. Syst. Charact. 10, 26–32.

Tingstad, J.E., Riegelman, S., 1970. Dissolution rate studies I: design and evaluation of a continuous flow apparatus. J. Pharm.Sci. 59, 692–696.

Tromelin, A., Gnanou, J.-C., Andrès, C., Pourcelot, Y., Chaillot, B., 1996. Study of morphology of reactive dissolution interface using fractal geometry. J. Pharm. Sci. 85, 924–928.

Yasuo, K., Kikuo, O., 1991. Particle size. In: Koichi, L., Keishi, G., Ko, H. (Eds.), Powder Technology Handbook. Marcel Decker, New York, pp. 3–14.